A numerical investigation of different touchdown patterns of thermal-flying-height-control sliders

Jinglin Zheng and David B. Bogy

Computer Mechanics Laboratory

Department of Mechanical Engineering, University of California at Berkeley, Berkeley, CA 94720

Zhengjinglin0420@berkeley.edu

Abstract

In this study we employ a numerical approach to explore the touchdown patterns of a thermal-flying-height-control (TFC) slider. Depending on the roughness of the head disk interface and thickness of the lubricant layer a TFC slider can experience different stages during touchdown. Three different touchdown patterns are shown. With a rougher interface profile, the slider smoothly transfers from a flying stage to a sliding stage. With an intermediate smooth interface profile, the slider experiences a flying-bouncing-sliding transition. With the smoothest interface, the slider goes through a flying-bouncing-surfing-sliding transition. Different stages are characterized by different slider dynamics and slider-disk contact status. The different touchdown dynamic patterns shown here can result in a significant difference in the easiness of successful touchdown detection. The general approach proposed here may also be applied to investigate the effects of other important head disk interface factors, e.g., air bearing surface design, heater, suspension, etc. on the slider's touchdown dynamic behaviors.

Keywords: *thermal flying-height control, touchdown dynamics, head disk interface*

Introduction

The ever-increasing demand for higher areal density in the magnetic recording hard disk drive industry has pushed the physical spacing between the recording head and media to ~1

nm (Marchon and Olson 2009). At this limit, the air bearing slider, which bears the read/write elements, is subject to various interfacial forces and experiences much more complicated dynamics. In this study we employ a numerical approach to explore the touchdown patterns of thermal-flying-height-control (TFC) sliders. Depending on the roughness of the head disk interface and thickness of the lubricant layer a TFC slider can experience different stages during touchdown. Three different touchdown patterns are shown. With a rougher interface profile the slider smoothly transfers from a flying stage to a sliding stage. With an intermediate smooth interface profile the slider experiences a flying-bouncing-sliding transition. With the smoothest interface the slider goes through a flying-bouncing-surfing-sliding transition. Different stages are characterized by different slider dynamics and slider-disk contact states. At the bouncing stage, the slider experiences strong vibrations and intermittent hard contacts with the disk, while the sliding stage is characterized by limited vibration amplitude and continuous slider-disk contact. At the so-called surfing stage (Liu et. al. 2009, Canchi and Bogy 2010, Chen et. al. 2012), which can exist between the bouncing and sliding stages, the slider experiences small vibrations and intermittent light contacts with the disk.

Numerical Model

A modified CML dynamic simulator is employed for this study in which the air bearing pressure solution is extended to contact conditions using a multi-asperity approach, and the effects of interfacial forces (contact, adhesion, friction and electrostatic forces) are included (Zheng and Bogy 2012a). A time-varying actuation profile is used as an input to bring the slider from flying to touchdown. A measured point-by-point disk profile is input as the waviness rotating with the disk (Zheng and Bogy 2012a). Three types of interfaces with key parameters listed in Table 1 are included in this study. In Table 1, the product of the standard surface heights σ, the radius of curvature R and the asperity areal density η is kept at ~0.05 to

make the surface "realistic" (Greenwood and Williamson 1966). The lubricant thickness t is fixed at 1.2 nm so that we can directly compare the flying height without considering the pushback due to different lubricant thicknesses. Other important interfacial parameters are listed in Table 2.

Table 1 Three sets of interface parameters

Standard deviation of surface heights σ (nm)	Asperity radius of curvature R (μm)	Asperity areal density η (μm^{-2})	Lube thick-ness t (nm)
0.6	0.5	133.33	1.2
0.5	0.5	159.68	1.2
0.35	0.5	200	1.2

Table 2 Other interfacial parameters for calculating interfacial forces (Suh and Polycarpou 2005)

Surface adhesion energy Δγ (N/m)	0.055
Disk Young's modulus (GPa)	280
Slider Young's modulus (GPa)	280
Disk Poisson ratio	0.24
Slider Poisson ratio	0.24
Disk hardness (GPa)	13
Potential difference between the head and disk (v)	0.5

Fig. 1 shows the normalized pull-off force as a function of the head disk spacing h for the three investigated cases listed in Table 1. The normalized pull-off force $F_{pull\text{-}off}$ is defined as

$$F_{pull-off} = \frac{F_c - F_s}{EA_n}$$

where F_c is the contact force, F_s is the adhesion force, E is the Hertz elastic modulus of the contacting surfaces and A_n is the nominal contact area. The head- disk spacing h is defined as the distance from the mean plane of the lubricant surface heights to the slider. With

decreasing *h* all three curves start from essentially zero and turn negative when the adhesion force becomes dominant. Further reduction in *h* leads to the domination of the contact force and this drives the pull-off force back to positive. The extent of the adhesion-dominant region and the minimum value of the pull-off force depend on the value of σ. A smaller σ in general leads to a steeper drop in the pull-off force at the adhesion-dominant region.

Result and discussion

The first touchdown pattern is obtained with an intermediate interface roughness (σ=0.5 nm). As shown in Fig. 2 the peak protrusion on the air bearing surface ramps up from 20 nm to 50 nm in a 10 ms time period to bring the slider from flying to touchdown. The corresponding flying height modulation at the transducer shows an instability region where the slider experiences obviously stronger dynamics. The time average of the transducer's FH shows that the slider continues penetrating deeper into the disk during this process.

Fig. 3 shows the contact force as a function of the peak protrusion where, by the features of the contact force curve, we can roughly divide the touchdown process into three stages: the flying stage during which the contact force is essentially zero, the bouncing stage where the contact force oscillates between zero and positive values, and the sliding stage where the contact force is always above zero. Comparing Figs. 2 and 3 we see that the bouncing stage corresponds to the instability region.

Fig. 4 shows the flying height 3σ and the average contact force as functions of the peak protrusion. At the flying stage the slider has a very limited modulation amplitude of ~0.5 nm, almost equal to the 3σ value of the disk profile, which means the slider almost perfectly follows the disk profile. When the slider is pushed to touchdown strong bouncing vibrations occur that bring the 3σ value to as high as ~1.5 nm, roughly 3 times that of the flying stage. Correspondingly, the average contact force jumps from 0 to ~0.4 mN. When the bouncing vibrations are damped and the slider gets out of the instability region the average contact

force remains stable temporarily. However, once the slider enters into the sliding stage, where its 3σ falls back to ~0.6 nm, the contact force starts increasing rapidly with the protrusion.

The second touchdown pattern is obtained with the roughest case (σ = 0.6 nm). The same actuation profile as shown in Fig. 2 is applied to the slider. As seen from Fig. 5 the touchdown process consists of two stages: the flying stage and the sliding stage. The slider's dynamics remains stable throughout the entire process with the 3σ value increasing from ~0.5 nm to ~0.6 nm after touchdown. In the meantime, the contact force increases rapidly with protrusion immediately after touchdown occurs.

The third touchdown pattern is obtained with the smoothest interface profile where σ equals 0.35 nm. As shown in Fig. 6 the slider experiences an instability region, which is similar to the first touchdown pattern. However, an extra stage, between the bouncing stage and the sliding stage, can be observed from the contact force curve. This stage is characterized by a small 3σ as well as minimum contact force, especially at the very beginning. We term this stage a "surfing" stage (Liu et. al. 2009, Canchi and Bogy 2010, Chen et. al. 2012) here because the flying height of the transducer is decreasing but there is little solid contact. So the only possibility is that the slider is in contact with the lubricant layer but barely touches the solid asperities beneath the lubricant.

Fig. 7 shows a comparison of the 3σ of the transducer's flying height for the three cases shown above. With a rougher interface profile, there is more stable dynamics of the slider, and for the roughest case, there is no instability region. Because the variation in the dynamics of the slider is commonly used in experiments to detect the occurrence of touchdown this result also indicates that it is more difficult to detect touchdown in rougher interfaces. From the spacing point of view, all three interfaces can maintain the slider at a stable read/write spacing for a flying height greater than ~ 0.5 nm. But in the two smoother cases the slider loses the stable read/write spacing when the minimum flying height drops below ~ 0.5 nm.

However, the slider comes back to a stable state when the minimum flying height is further reduced to less than ~ -0.5 nm. But as can be seen from Fig. 8, the slider experiences a much stronger contact force in the roughest interface but essentially zero contact force in the smoothest interface, which suggests a potential for ultra-low operating flying height with the smoothest interface.

Because the adhesion force is a potential source for inducing the bouncing vibrations at touchdown (Zheng and Bogy, 2012b) we can interpret the touchdown patterns obtained here with different interface roughnesses from the behaviors of adhesion forces for the three investigated cases. Fig. 9 shows the asperity height distribution function $\phi(u)$, which is Gaussian, for two interface profiles: the one on the first row represents a rough interface where $\phi(u)$ spreads in a wider range of asperity heights, the one on the second row represents a smooth interface where $\phi(u)$ is concentrated in a narrow range of asperity heights. For a given head-disk separation d (defined from the mean plane of the solid surface heights, which is offset from the mean plane of the lubricant surface heights by t, namely, $d = h + t$), asperities higher than d are in solid-contact status, asperities higher than d-t but lower than d are in lubricant-contact status, and the rest of the asperities are in non-contact status.

Referring to the first column in Fig. 9 we see that at a higher separation d_1, which corresponds to a higher flying height, due to the existence of high asperities in the rough interface, some adhesion is generated at the high asperities. But this adhesive effect is weak because of the limited number of high asperities. On the other hand, almost all asperities in the smooth interface are too far away to cause any significant adhesive effect on the slider. As the separation reduces from d_1 to d2 (the second column in Fig. 8), for the rough case, the number of lubricant-contact asperities quickly increases and occupies a large area beneath $\phi(u)$, and this causes a strong adhesion force. But solid contact bonds are also created at some high asperities, resulting in a supportive force that adds to the air bearing lift and offsets the adhesive effect. For the smooth interface the adhesion force quickly increases to a maximum

because most asperities are at approximately the same height and are close enough to generate strong adhesive effects. As a result, a slider in a smooth interface is likely to experience large bouncing vibrations due to this rapidly increasing adhesion force. As the separation further reduces to d_3 (the third column in Fig. 9) it is seen that the percentage of solid-contact asperities quickly increases in the rough case, which further suppresses the effects by adhesion. However, because of the high ratio of t/σ, the percentage of asperities causing adhesion barely changes from the separation d_2 to d_3, for the smooth case. On the other hand, the percentage of solid-contacting asperities is still too small to cause any significant contact force. Thus the slider is likely to return to stable dynamics, and this may result in a surfing stage.

It should be noted that although the numerical model here predicts a stable state of the slider at the surfing stage, the feasibility of recording at the surfing stage is still questionable because the interaction between the slider and the disk lubricant can cause other issues, like disturbances to the lubricant surface profiles, contamination on the air bearing surface, etc. These problems can prevent the slider from maintaining a stable read/write spacing while being in contact with the lubricant.

Conclusion

Different touchdown patterns characterized by different stages of contact can be achieved by modifying the roughness of the head disk interface. A rougher interface leads to more stable touchdown dynamics and even elimination of bouncing vibrations whereas a smoother interface may result in a surfing stage between the bouncing and sliding stages, which is characterized by stable dynamics as well as minimized solid contact.

References

Canchi SV and Bogy DB (2010) Slider Dynamics in the Lubricant-Contact Regime. IEEE Trans Magn 46: 764-769

Chen YK, Zheng J, Bogy DB (2012) Light contact and surfing state dynamics of air bearing sliders in hard disk drives. Appl Phys Lett 100: 243104. doi: 10.1063/1.4729055

Greenwood JA and Williamson JBP (1966) Contact of nominally flat surfaces. Proc R Soc Lond A Math Phys Sci 295: 300-319

Liu B, Zhang MS, Yu SK, Hua W, Ma YS, Zhou WD, Gonzaga L, Man YJ (2009) Lube-Surfing recording and its feasibility exploration. IEEE Trans Magn 45: 899-904

Marchon B and Olson T (2009) Magnetic spacing trends: from LMR to PMR and beyond. IEEE Trans Magn 45: 3608-3611

Suh AY and Polycarpou AA (2005) Adhesive contact modeling for sub-5-nm ultralow flying magnetic storage head-disk interfaces including roughness effects. J Appl Phys 97:104328

Zheng J and Bogy DB (2012a) Dynamic instability of thermal-flying-height-control sliders at touchdown. Microsyst Technol. doi: 10.1007/s00542-012-1537-6

Zheng J and Bogy DB (2012b) Numerical simulation of touchdown Dynamics of thermal flying-height control sliders. IEEE Trans Magn: accepted

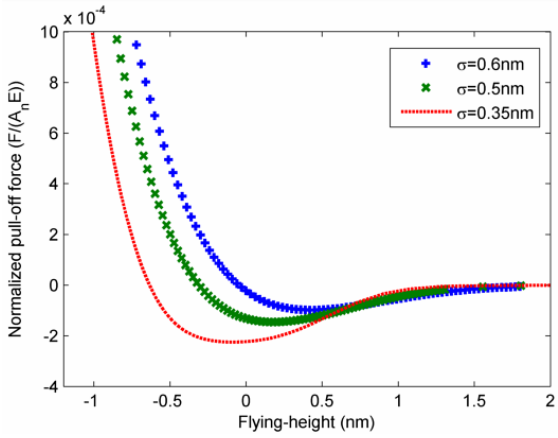

Fig. 1 Normalized pull-off force as a function of the head disk spacing *h* for the three cases listed in Table 1.

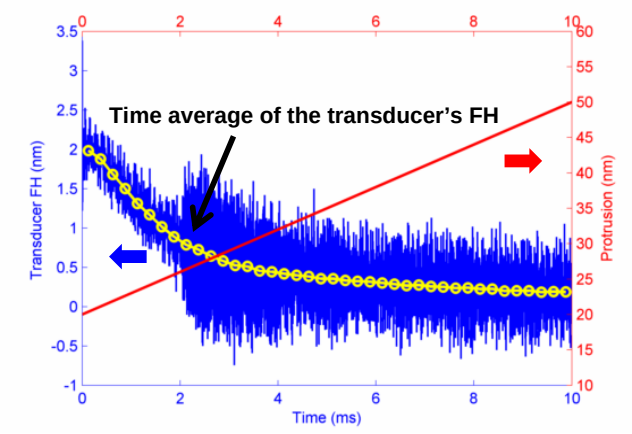

Fig. 2 Peak protrusion on the slider and the transducer's flying height as functions of time for the case σ = 0.5 nm.

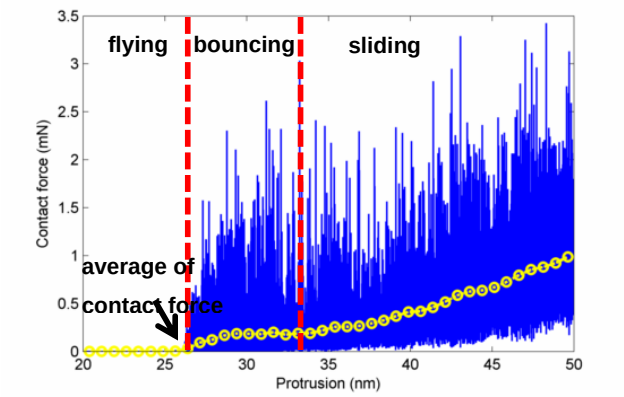

Fig. 3 Contact force acting on the slider as a function of the peak protrusion for the case σ = 0.5 nm.

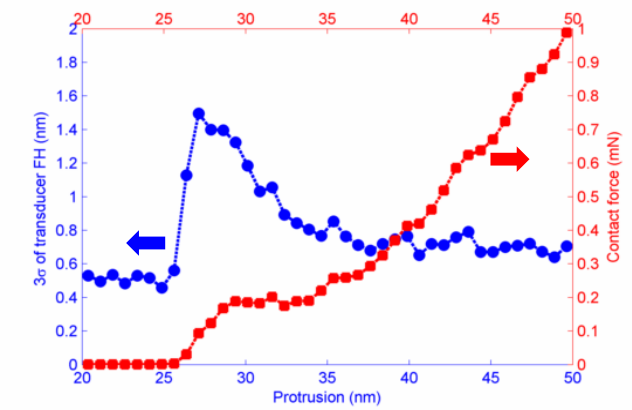

Fig. 4 3σ of the transducer's FH and average contact force as functions of the peak protrusion on the slider for the case σ = 0.5 nm.

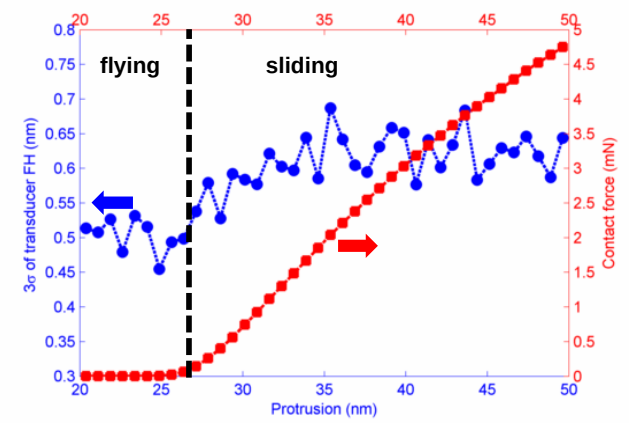

Fig. 5 3σ of the transducer's FH and average contact force as functions of the peak protrusion on the slider for the case σ = 0.6nm.

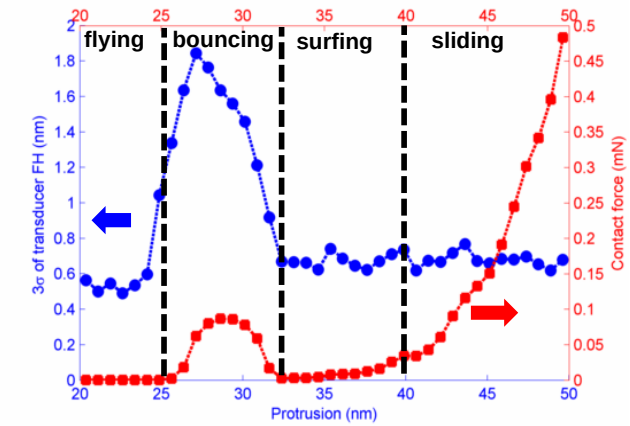

Fig. 6 3σ of the transducer's FH and average contact force as functions of the peak protrusion on the slider for the case σ = 0.35nm.

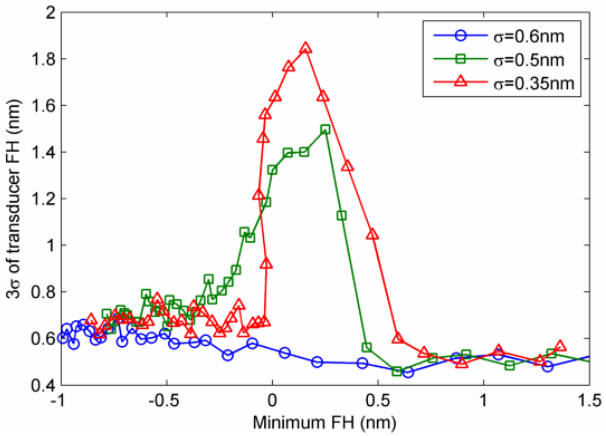

Fig. 7 3σ of the transducer's FH as a function of the minimum flying height.

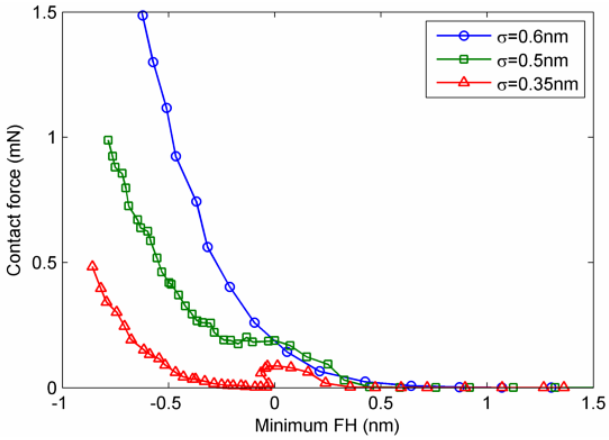

Fig. 8 Average contact force as a function of the minimum flying height.

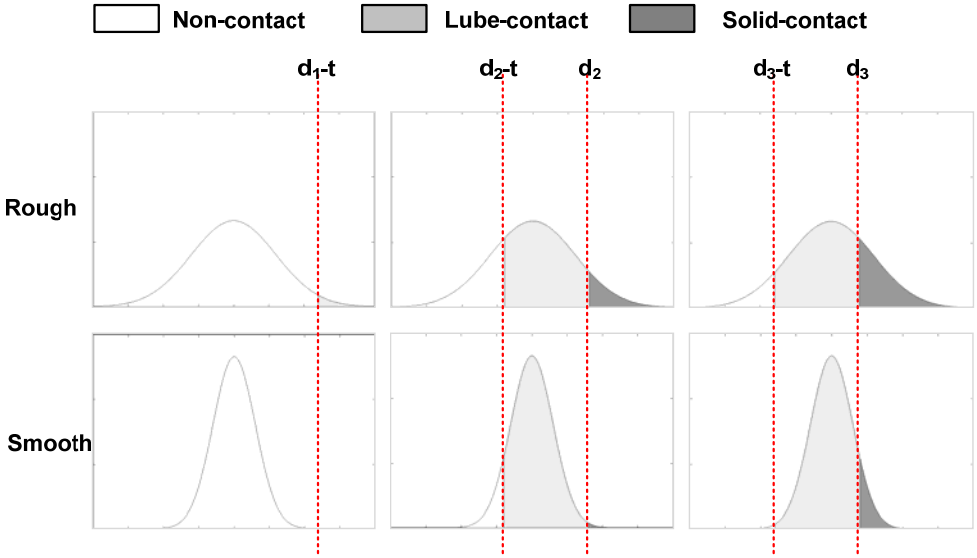

Fig.9 the asperity height distribution function ϕ(u) for a rough interface profile (top row) and a smooth interface profile (bottom row).